文章编号：1000-8608(2011)04-0498-07

Effect of cold spray particle conditions and optimal standoff distance on impact velocity

WANG Xiao-fang*[1], YIN Shuo[1], XU Bao-peng[2]

(1. School of Energy and Power Engineering, Dalian University of Technology, Dalian 116024, China;
2. Faculty of Engineering, Kingston University, London SW15 3DW, England)

Abstract: The impact velocity of particles plays an important role in coating formation of cold spray. A proper standoff distance from the nozzle exit to the substrate surface can ensure sprayed particles to achieve relatively high impact velocities. Numerical simulations were conducted by using a CFD software, Fluent, to predict the supersonic flow field outside the nozzle. Based on the simulation results, the effect of particle conditions on impact velocity is studied and also the way to determine the optimal standoff distance is proposed. It is found that particles with small size, low density or irregular shape can be significantly affected by the dilatational waves, oblique shock waves and bow shock waves. With the energy dissipation or passing through the bow shock waves, these particles are decelerated sharply. Moreover, there exists an optimal standoff distance for different conditions. The determination of the optimal standoff distance requires two essential considerations: One is that the substrate must be located at the place where the carrier-gas velocity is relatively low to weaken the strength of the bow shock waves; the other is that particles should be accelerated twice by dilatational waves before entering the bow shock waves, which means there must be two groups of dilatational waves in front of the bow shock waves.

Key words: cold spray; numerical simulation; bow shock waves; optimal standoff distance

0 Introduction

Cold spray, also called cold gas-dynamic spray (CGDS), is radically different from conventional thermal spray methods. The deposition process relies purely on kinetic energy rather than the combination of thermal and kinetic components. In this process, spray particles (generally <50 μm) are accelerated to a high velocity (ranging from 300 to 1 200 m/s) by the supersonic gas flow which is generated in the convergent-divergent de Laval nozzle [1-4]. A coating is formed through the intensive plastic deformation of particles impacting upon a substrate at a temperature well below the melting point of spray material [5,6]. Generally, there exists a critical velocity for a given spray material, at which the transient from erosion of substrate to particle deposition takes place [2-6]. Only if the particle impact velocity is above the critical value, could the coating be formed. Cold spray has many advantages, such as the wider choices of metals and alloys as coating materials,

Received by: 2009-08-20; **Revised by**: 2011-05-25.
Supported by: "973" National Basic Research Program of China (Grant No. 2009CB724303); National Natural Science Foundation of China (Grant No. 50476075); Chinese Ministry of Education's Academic Award for Outstanding Doctoral Student.
Corresponding author: WANG Xiao-fang* (1960-), Female, Prof., Supervisor of Doc., E-mail: dlwxf@dlut.edu.cn.

the capability of oxygen-free coating and high deposition efficiency [4,7-10]. It has attracted more and more attentions now.

During the past decade, several researchers had focused on the effect of particle conditions on its acceleration behavior inside and outside the nozzle. Jen, *et al*. [11] reported that the bow shock waves almost had no effect on copper particles of more than 5 μm and significantly affected the particles less than 1 μm through CFD simulations. Li, *et al*. [12] further showed that particles with smaller size, lower density or more irregular shape were easier to be accelerated by the carrier-gas via numerical method. Pattison, *et al*. [13] confirmed this using the experiment in a free jet. However, a systemic investigation on effect of particle size, density and shape on its impact velocity, which is the most important factor in cold spray process, is still lacking.

For the optimal standoff distance, there have been very little literatures concerning this research. Gilmore, *et al*. [4] sprayed copper particles with helium and found that particle velocity only began to decrease when the standoff distance was more than 50 mm. Stoltenhoff, *et al*. [14] gave a proof to this observation by using numerical simulation. Pattison, *et al*. [13] employed the experimental method to point out that there exists an optimal region in which the deposition efficiency can reach a high value. Although some reports referred to the standoff distance in cold spray, the reason why the optimal standoff distance exists and how to determine it are still not well understood.

Therefore, in this study, the numerical method was employed to give a detailed investigation into the effect of particle conditions on its impact velocity, and examine the determination of optimal standoff distance.

1 Mathematical modeling

1.1 Numerical modeling

Numerical modeling is performed by using the CFD software Fluent to determine the flow field of free jet and impact jet outside the nozzle. The gas is taken as an ideal and compressible one. A coupled implicit method is used to solve the flow field and the result of flow field in a steady state is obtained. The standard K-ε turbulence model available in Fluent is utilized for modeling the turbulent flow in the simulation. The accelerating of particles is computed using discrete phase modeling (DPM). The interaction of particle with gas is not considered in this study. The governing equations for gas flow include the physical laws of conservation of mass, momentum, and energy. Models describing the dynamic behavior of in-flight particles during the two-phase flow have been well documented in the Fluent manual[15].

1.2 Geometrical model and boundary conditions

Owing to the axisymmetrical characteristics of the flow field in this study, a two-dimensional symmetrical model is employed as shown in Fig. 1. The diameter of the nozzle exit is chosen as 4 mm. Pressure-based boundary conditions are applied to the inlet and outlet, while no-slip condition and a fixed heat flux of zero are enforced at the nozzle wall and substrate. The atmosphere is treated as non-reflecting

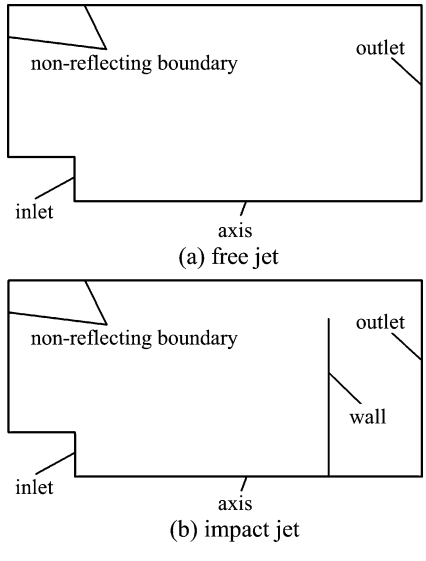

Fig. 1　Schematic diagram of the computational domain and boundaries of the free jet and the impact jet

boundary. The meshing is conducted with the quad elements. The initial velocity of the carrier-gas has been set as 617 m/s at the nozzle exit according to the authors′ previous experimental results. Moreover, it is assumed that the initial velocity of particles is defined as the same value as that of the carrier-gas in order to ensure that all the particles have a same initial condition at the nozzle exit and make the comparison much clearer.

2 Results and discussion

2.1 Gas flow field in the free jet

Fig. 2 illustrates the pressure profile in the free jet by using air as carrier-gas in order to find the general flow feature of free jet flow field. A well-formed complex wave structure can obviously be seen, where dilatational waves and oblique shock waves appear alternately. The first region near the nozzle exit presents several dilatational waves owing to the non-ideally expanding with a rapid acceleration of gas velocity and then presents compression waves as a result of the reflection at the atmosphere boundary. These compressional waves are combined to the oblique shock wave to reduce the flow velocity with increasing the pressure and the temperature sharply. The periodic variation of the wave structure results in the fluctuation of carrier-gas velocity at the centerline. Furthermore, it is also noticed that the oscillation amplitude of this complicated wave structure is reduced gradually along the jet direction because of the viscous dissipation. Eventually, the flow energy is dissipated and stabilized to the environmental pressure through continuous adjustment of the supersonic flow.

Fig. 3 shows the velocity plot of carrier-gas along the nozzle centerline. It is clear that the gas velocity experiences a periodic fluctuation along the centerline in the form of a rapid increase followed by a steep decrease. The carrier-gas has been accelerated through the dilatational wave, and then starts to decrease

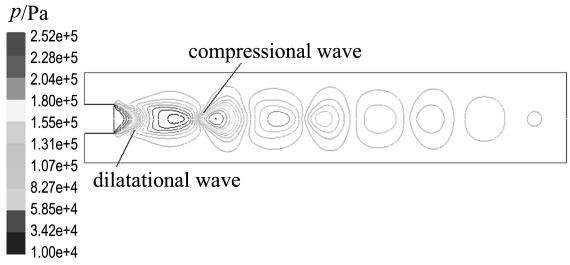

Fig. 2 Pressure profile outside the nozzle in the free jet using air as carrier-gas at a pressure of 0.252 MPa and a temperature of 300 K

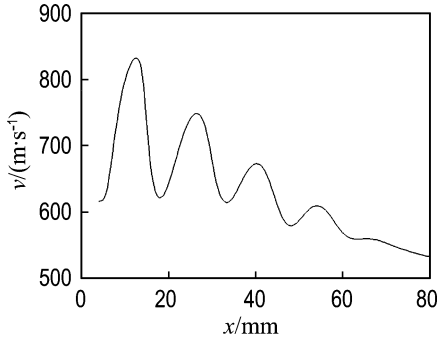

Fig. 3 Velocity plot of carrier-gas along the nozzle centerline

when penetrating into the oblique shock wave until the next expansion wave comes. Moreover, the maximum gas velocity is about 840 m/s at the location of 12 mm from the nozzle exit after the first dilatational wave and the subsequent peak values decrease gradually. The velocity distribution can be well explained by the wave structure shown in Fig. 2. Jodoin, *et al*. [16] also reported the same phenomenon through experiments using nitrogen as carrier-gas at the stagnation pressure of 2.4 MPa and temperature of 733 K.

2.2 Effect of particle size, density and shape on particle impact velocity

Following the free jet study, impact jet is simulated to clarify the effect of particle size, density and shape on particle impact velocity. Fig. 4 exhibits the pressure profile in the impact jet with the substrate 16 mm away from the nozzle exit by using air as carrier-gas. It is obvious that the existence of the substrate causes the wave structure more different from that in the free jet. The obvious dilatational

waves are seen outside the nozzle exit, followed by the oblique shock waves. Between the nozzle exit and the substrate, there exists a well-formed bow shock wave located close to the substrate, which arises from the interaction between the gas flow and the substrate. The pressure in this region is well confined, leading to a much higher pressure increase at the substrate and a significantly different flow pattern. The flow velocity decreases rapidly to nearly zero when the gas flow penetrates into the bow shock wave and approaches the substrate.

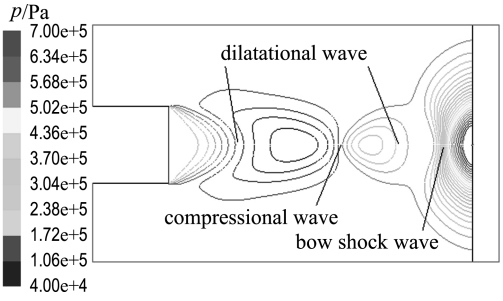

Fig. 4　Pressure profile outside the nozzle using air as carrier-gas with the substrate 16 mm away from the nozzle exit at a pressure of 0.252 MPa and a temperature of 300 K

Fig. 5 compares the impact velocities of spherical copper, titanium and aluminum particles in order to find the effect of material density on particle impact velocity. The densities of aluminum, titanium and copper powders are 2 719, 4 850 and 8 978 kg/m^3, respectively. It is apparent that three types of particles almost have the same velocity changing tendency. Aluminum particle with the lowest density is more susceptible to carrier-gas than the other two particles. Therefore, it is easily picked up and accelerated to the highest velocity before entering into the bow shock wave. However, when penetrating into the bow shock waves, aluminum particle is also easily decelerated and the velocity drops steeply from the highest value of nearly 640 m/s to the lowest value of about 610 m/s, while titanium particle and copper particle achieve relatively higher impact velocities due to their large densities. Moreover, in order to examine the influence of particle shape on the particle impact velocity, the comparison of spherical and non-spherical titanium particles with the equivalent diameter of 5 μm is also given in Fig. 5. It is easily found that the non-spherical titanium particle has a higher velocity before penetrating into the bow shock waves, but a lower impact velocity. This fact can be linked to the morphologies of particles. The drag coefficient of a sphere particle is less than that of an equivalent diameter but irregular shape particle. Therefore, the non-spherical titanium particle can be easily picked up by the gas flow and also seriously affected by the bow shock waves.

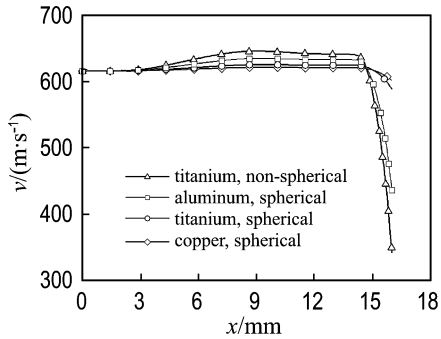

Fig. 5　Comparison of velocities of spherical copper, titanium, aluminum particles and non-spherical titanium at the standoff distance of 16 mm along the nozzle centerline

Fig. 6 shows the centerline velocity of copper particles with different diameters in the impact jet. Small particle is easily picked up through the drag force of carrier-gas compared with large one. However, as the particles traverse the bow shock waves, the acceleration suddenly becomes deceleration. When coming to the bow shock waves, large particles are affected slightly by the drag force and maintain sufficient impact velocity as a result of the significant momentum and energy. On the contrary, small and light particles are decelerated steeply by the

bow shock waves although they can be accelerated greatly by the carrier-gas before entering the bow shock waves. The final impact velocities of copper particles with different diameters are displayed in Fig. 6. It gives a clear suggestion that the larger particle can achieve a higher impact velocity when impacting the substrate. It is clearly found that with increasing the particle size, the effect of gas flow becomes slight and the impact velocity rises gradually. Jen, *et al*.[11] also reported that the bow shock waves almost had no effect on copper particle with a diameter larger than 5 μm and significantly affected the particle with a diameter less than 1 μm.

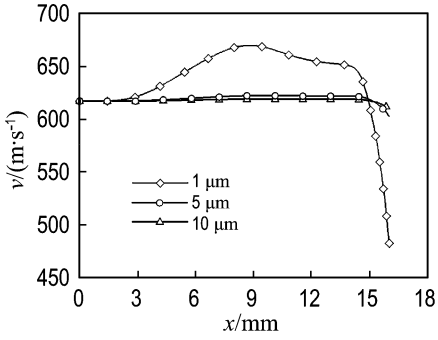

Fig. 6 Comparison of velocity of copper particles with different diameters at the standoff distance of 16 mm along the nozzle centerline

2.3 Optimal standoff distance

Fig. 7 shows the effect of standoff distance (d) on impact velocity by using copper particles with different sizes. It is clearly observed that there exists an optimal standoff distance between the nozzle exit and the substrate. Under the given condition in this study, the optimal distance is 16 mm. The reason for this is that the carrier-gas velocity at 16 mm is the lowest in the first changing period in the free jet as shown in Fig. 3. Therefore, when setting the substrate at this position, the intensity of the bow shock waves must be very small, which could weaken the deceleration effect of the bow shock waves on particle impact velocity and thus particle can achieve a higher impact velocity. However, it also can be noticed that in the free jet there exist several velocity changing periods and each has a minimum point of gas velocity. Thus, it can be deduced that there must be another limitation to determine the optimal standoff distance of 16 mm. In order to find this determinant, the standoff distance of 32 mm is chosen. The carrier-gas velocity at this distance is the lowest in the second changing period in the free jet. Fig. 8 shows pressure profile outside the nozzle using air as carrier-gas with the substrate 32 mm away from the nozzle exit at a pressure of 0.252 MPa and a temperature of 300 K. It can be seen that the particle experiences twice acceleration and three times deceleration before entering into the bow shock waves due to the alternant

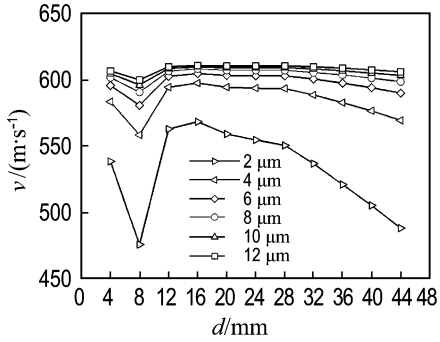

Fig. 7 Effect of standoff distance on impact velocity by using copper particles with different diameters

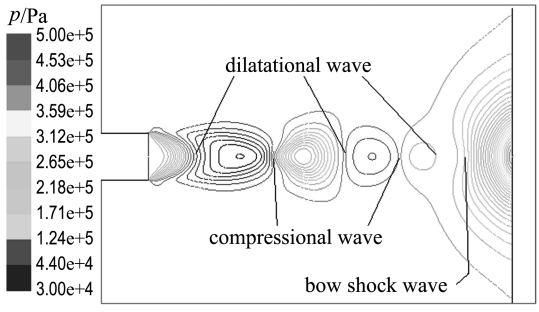

Fig. 8 Pressure profile outside the nozzle using air as carrier-gas with the substrate 32 mm away from the nozzle exit at a pressure of 0.252 MPa and a temperature of 300 K

dilatational waves and oblique shock waves. After the second dilatational wave, the deceleration effect of drag force becomes more intensive than the positive drag force as a result of the energy dissipation in carrier-gas. Therefore, the in-flight particle velocity can not reach the peak before permeating into the bow shock waves. However, when the standoff distance is 16 mm as shown in Fig. 5, the particle experiences twice acceleration and only once deceleration. The particle uses the positive drag force effectively to obtain a higher velocity compared with that the standoff distance is 32 mm.

From the discussion above, it can be easily concluded that the determination of the optimal standoff distance needs two essential conditions to ensure that the particle can achieve the highest impact velocity. The first one is that the substrate must be located at the place where the carrier-gas velocity is lower in the free jet. The other is that the particles should be accelerated twice before entering the bow shock wave, which means there must be two dilatational waves in front of the bow shock wave. The previous experimental study on the standoff distance conducted by Pattison, *et al*.[13] also reported the similar results that the optimal standoff distance in cold spray linked closely to the bow shock wave intensity. Only for the proper standoff distance at which the bow shock wave intensity is weak, the particle impact velocity and the deposition efficiency can reach a higher value. Also, Li, *et al*. [17] reported the same phenomenon that standoff distance actually affected the impact velocity and the optimal standoff distance indeed existed in cold spray by experiment method. These facts further enhance the value of this study.

3 Conclusions

(1) Particle size, density and shape play critical roles in in-flight particle velocity and impact velocity. Particles with small size, low density or irregular shape can be easily affected by the carrier-gas. These particles can be accelerated to a higher velocity by the positive drag force and decelerated sharply by viscous dissipation and the bow shock wave. But large size, high density or spherical particle is not sensitive to the carrier-gas and thus can obtain a higher impact velocity while impacting the substrate.

(2) The existence of the substrate causes the wave structure more different from that in the free jet. The obvious bow shock wave which arises from the interaction between the gas flow and the substrate, leading to a steep deceleration of particle velocity.

(3) There exists an optimal standoff distance. The determination of this distance requires two conditions. The first one is that the substrate must be located at the place where the carrier-gas velocity is lower. The other is that particles should be accelerated twice before entering the bow shock wave, which means there must be two dilatational waves in front of the bow shock wave.

References:

[1] ALKIMOV A P, KOSAREV V F, PAPYRIN A N. A method of cold gas-dynamic deposition [J]. **Doklady Akademii Nauk SSSR**, 1990, **318**(5): 1062-1065

[2] DYKHUIZEN R C, SMITH M F. Gas dynamic principles of cold spray [J]. **Journal of Thermal Spray Technology**, 1998, **7**(2): 205-212

[3] ASSADI H, GARTNER F, STOLTENHOFF T, *et al*. Bonding mechanism in cold gas spraying [J]. **Acta Materialia**, 2003, **51**(15): 4379-4394

[4] GILMORE D L, DYKHUIZEN R C, NEISER R A, *et al*. Particle velocity and deposition efficiency in the cold spray process [J]. **Journal of Thermal Spray Technology**, 1999, **8**(4): 576-582

[5] PAPYRIN A. Cold spray technology [J]. **Advanced Materials and Processes**, 2001, **159**(9): 49-51

[6] KARTHIKEYAN J. Cold spray technology [J]. **Advanced Materials and Processes**, 2005, **163**(3):33-35

[7] STEENKISTE T V, SMITH J, TEETS R. Aluminum coatings via kinetic spray with relatively large powder particles [J]. **Surface and Coatings Technology**, 2002, **154** (2-3):237-252

[8] LI C J, LI W Y. Deposition characteristics of titanium coating in cold spraying [J]. **Surface and Coatings Technology**, 2003, **167**(2-3):278-283

[9] KIM H J, LEE C H, HWANG S Y. Fabrication of WC-Co coatings by cold spray deposition [J]. **Surface and Coatings Technology**, 2005, **191** (2-3):335-340

[10] LI W Y, LI C J, WANG Y Y, *et al*. Effect of Cu particle parameters on its impacting behavior in cold spraying [J]. **Acta Metallurgica Sinica**, 2005, **41**(3):282-286 (in Chinese)

[11] JEN T C, LI L J, CUI W Z, *et al*. Numerical investigations on cold gas dynamic spray process with nano- and microsize particles [J]. **International Journal of Heat and Mass Transfer**, 2005, **48** (21-22):4384-4396

[12] LI W Y, LI C J. Optimization of spray conditions in cold spraying based on the numerical analysis of particle velocity [J]. **Transactions of Nonferrous Metals Society of China**, 2004, **14**(s2):43-48

[13] PATTISON J, CELOTTO S, DHAN A, *et al*. Standoff distance and bow shock phenomena in the cold spray process [J]. **Surface and Coatings Technology**, 2008, **202**(8):1443-1454

[14] STOLTENHOFF T, KREYE H, RICHTER H J. An analysis of the cold spray process and its coatings [J]. **Journal of Thermal Spray Technology**, 2002, **11**(4):542-550

[15] Fluent Inc.. FLUENT 6.1 User's Guider [Z]. Lebanon:Fluent Inc., 2003

[16] JODOIN B, RALETZ F, VARDELLE M. Cold spray modeling and validation using an optical diagnostic method [J]. **Surface and Coatings Technology**, 2006, **200**(14-15):4424-4432

[17] LI W Y, ZHANG C, GUO X P, *et al*. Effect of standoff distance on coating deposition characteristics in cold spraying [J]. **Materials and Design**, 2008, **29**(2):297-304

冷喷涂粒子性状及基板最佳位置对冲击速度影响

王晓放*[1], 殷 硕[1], 徐宝鹏[2]

(1.大连理工大学 能源与动力学院,辽宁 大连 116024;
2.金斯顿大学 工程学院,英国 伦敦 SW15 3DW)

摘要: 冷喷涂中,粒子撞击基板时的速度对涂层形成起到至关重要的作用,而适当的喷涂距离可以使喷涂粒子获得较高的速度.利用商用 CFD 软件 Fluent 模拟了喷嘴外超音速流场的分布情况,分析了粒子自身条件对冲击速度的影响,同时提出了确定粒子与基板最佳距离的方法.分析发现,小尺寸、低密度以及不规则形状的粒子容易受到喷嘴外产生的膨胀波、斜激波和基板前的弓形激波影响.随着能量的耗散或当粒子穿过弓形激波时,这些粒子的速度明显下降.另外,在基板与喷嘴之间存在一个最佳距离,它的确定需要两个必要条件:一是基板处的气流必须保持较低的速度,从而使弓形激波的强度相对较弱;二是粒子须经膨胀波加速 2 次,即弓形激波前具有 2 个膨胀波,以确保气体可充分利用膨胀波的加速.

关键词: 冷喷涂;数值模拟;弓形激波;基板最佳距离

中图分类号: TQ63;TG174 **文献标志码:** A

收稿日期: 2009-08-20; **修回日期:** 2011-05-25.

资助项目: "九七三"国家重点基础研究发展计划资助项目(2009CB724303);国家自然科学基金资助项目(50476075);教育部博士研究生学术新人奖资助项目.

作者简介: 王晓放*(1960-),女,教授,博士生导师,E-mail:dlwxf@dlut.edu.cn.